Pulliam [15], need to be developed and refined. The proper way to handle this is to divide memory into two parts, the operating part of memory and the storage part. Identifiable blocks of data are brought into the working area, processed and then moved back to storage. There are a number of advantages to such a system. One is that large blocks of data can be moved more efficiently especially for out-of-core storage devices but even for in-core storage. The dimensions of the blocks define the vector lengths. For SIMD (single instruction - multiple data) or MIMD (multiple instruction - multiple data) architecture the blocks define multiple data strings to be operated on. In general, as machines become larger and more powerful we will have to take more care in the development of a well structure efficient code.

12.5 Application in Three Dimensions

Applications in three dimensions require substantial computational resources. Most of the problems attempted so far have been for simple geometries and limited flow conditions. The advent of the high speed – large memory machines, such as the CRAY 1S, XMP or CYBER 205, will enable us to attempt realistic problems but even they fall short of providing enough computer power for general purposes. I shall present below applications of the code ARC3D for simple body shapes. The flow conditions used, though, produce some interesting and complicated flowfields. These computations demonstrate the capabilities of the code and demonstrate the accuracy and efficiency.

A) Hemisphere-Cylinder At High Angle Of Attack

The first application is flow past a semi–infinite hemisphere–cylinder at a supersonic Mach number $M_\infty = 1.2$ and high angle of attack $\alpha = 19°$. The calculation is for a laminar Reynolds number $RE = 222500.0$ This calculation was originally presented by Pulliam and Steger [3] where it was computed on a grid with 30 points in the axial direction , 19 points circumferentially and 30 points in the normal direction, a total of 17100 grid points. The grid is a warped spherical topology, see Fig. 31 and is clustered in the normal direction for boundary layer resolution. In the original code [3] the convergence rate (reduction in residual per iteration) for typical cases was on the order of 0.996, for the current algorithm it has been reduced to approximately 0.986. Employing the algorithm as described above and using the fully implicit pentadiagonal algorithm the computation time for three orders of magnitude drop in residual (plotting accuracy) was reduced from about 300 minutes for a converged case on the CDC7600 to about 5 minutes on a CRAY-XMP. In fact cases which could not be converged before on the CDC 7600 are now convergent. This is a substantial reduction in the compute time and can be improved further.

An example of the computation is shown in Fig. 32 and 33. A crossflow separation occurs at this angle of attack which is indicated by the pressure contours and velocity vectors at the cross sectional plane shown. In Fig. 33 pressure along

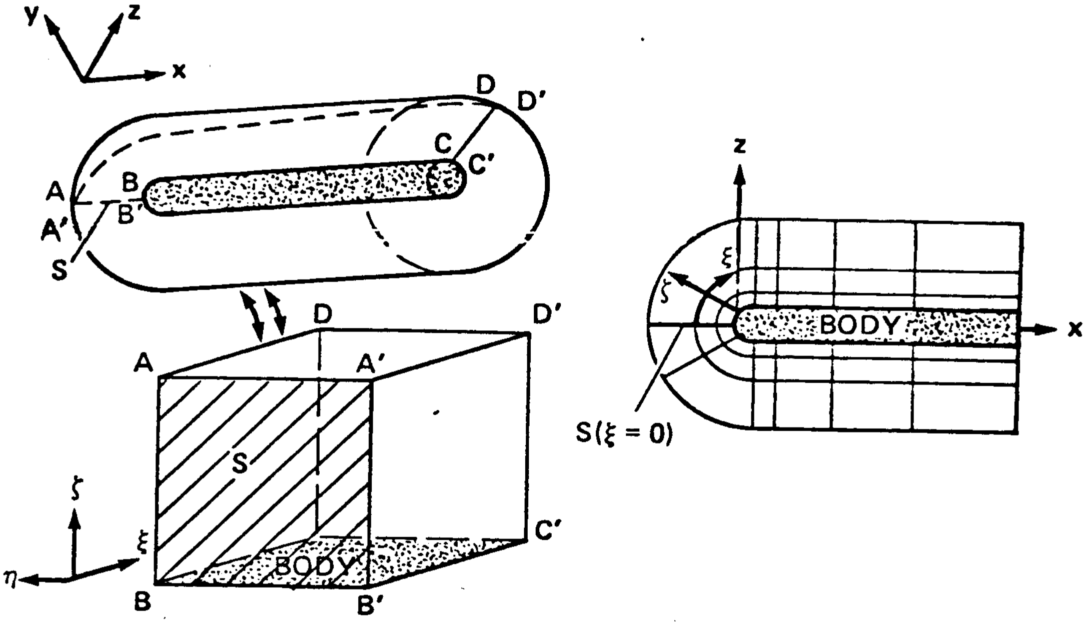

FIGURE 31. Warped Spherical Topology for Hemisphere–Cylinder.

the body at three circumferential locations is compared with experimental data due to Hsieh [61] and compares quite well. Also shown is the computed crossflow separation angle against experiment.

Details of the interaction of the crossflow and symmetry plane as well as other features of this flow require further study. Results by Pan and Pulliam [46] have expanded ARC3D to use the SSD (solid state disk) on the XMP. This give us the capacity for up to 1 million grid points. With that resolution and the increase efficiency of the code we are carring out a detailed study of high angle of attack flowfields.

Other computations presented for this configuration at lower Mach numbers and angles of attack were reported by Pulliam and Steger and compared well with data. The code is also used to obtain starting solutions for a PNS (parabolized Navier-Stokes) code, see Schiff and Steger [62], Chaussee, et. al. [63].

B) Boattail

As a second application, Deiwert employed a version of the code to study boattails at angles of attack [64] and boattail exhaust plumes [65]. A composite of Deiwerts boattail computation is given in Fig. 34. The computation was performed using a boattail configuration with a infinite sting. The region of interest is the converging area of the boattail. The flow conditions are $M_\infty = 2.0$, $Re = 6.5 \cdot 10^7$ and angles of attack from $0°$ to $12°$. Computed pressures at various angles of attack

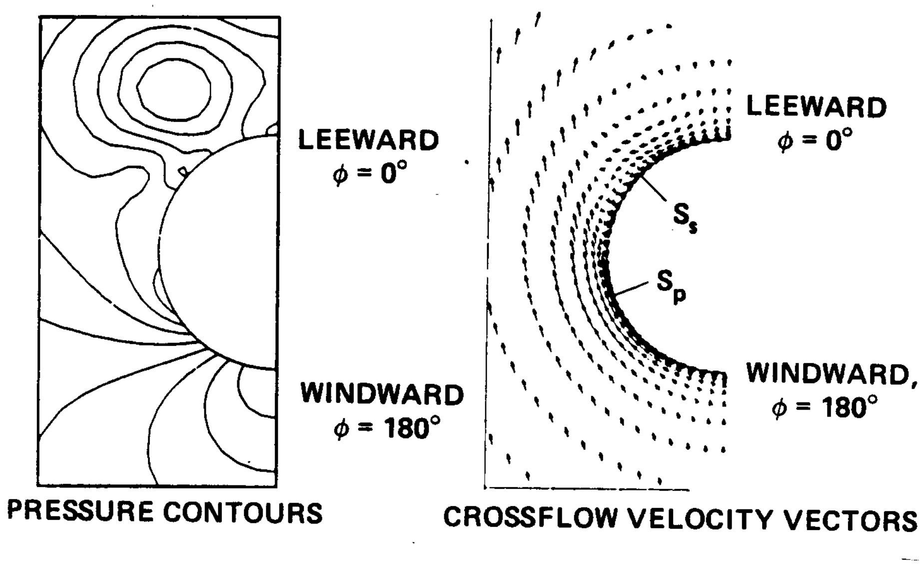

FIGURE 32. Hemisphere–Cylinder at $M_\infty = 1.2, \alpha = 19°$.

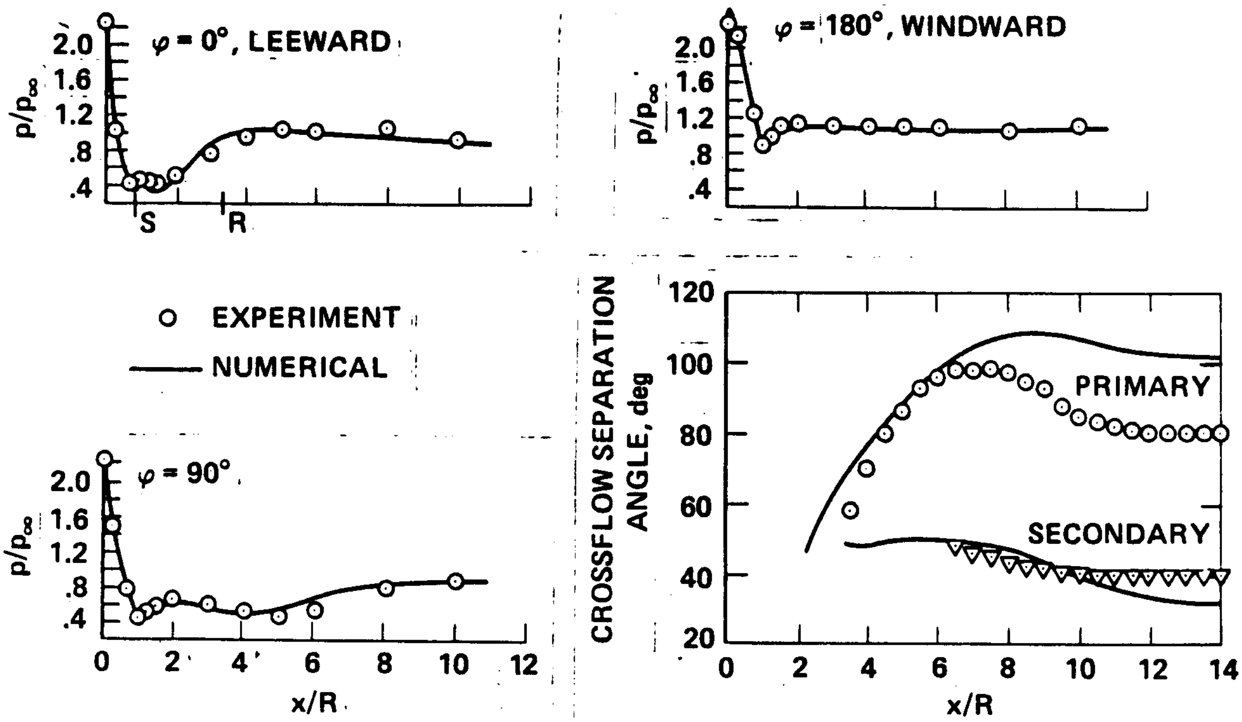

FIGURE 33. Comparison with Experiment.

are compared with experiment in the paper. The case shown here is for $\alpha = 6°$ and shows comparison at three circumferential stations. Computed surface oil flow (particle paths restricted to the body) and surface pressure for $\alpha = 6°$ show the type of results presented. The results reported by Deiwert [64] compared very well with the experimental data of Shrewsbury [66].

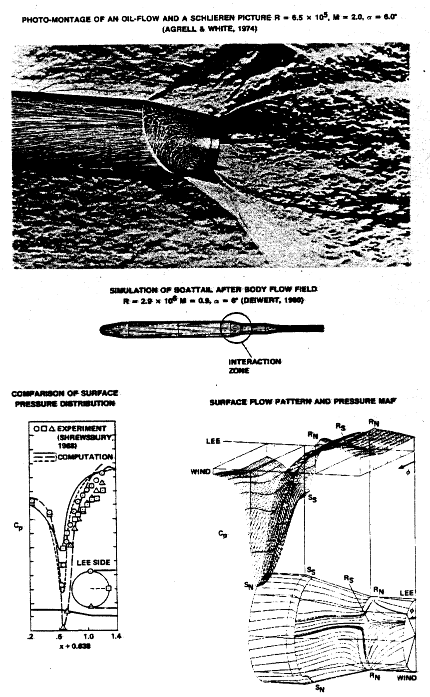

FIGURE 34. Boattail Study at $M_\infty = 2.0, \alpha = 6°, Re = 6.5 \times 10^5$.

The boattail study was undertaken as a first step toward the simulation of boattail exhaust plumes which has been carried out in a preliminary stage by Deiwert [65]. In this simulation the boattail sting is eliminated and a conical exhaust jet is added at the base region. Figures 35 and 36 show comparisons of density contours and streamlines with Schlieren photographs from Agrell and White [67]. In Fig. 35 the pressure ratio for the jet was 3 and we see an expanded exhaust plume and a complicated shock shear flow pattern (depicted by the bold lines). The qualitative comparison with the photograph is quite remarkable. At a higher exhaust ratio, Fig. 36 the jet is tighter and the shock shear surface pattern more complicated. Again the qualitative comparison with the photograph is quite good. I refer the reader to the original papers and one by Nakahashi and Deiwert [60] for a more detailed analysis of these flowfields.

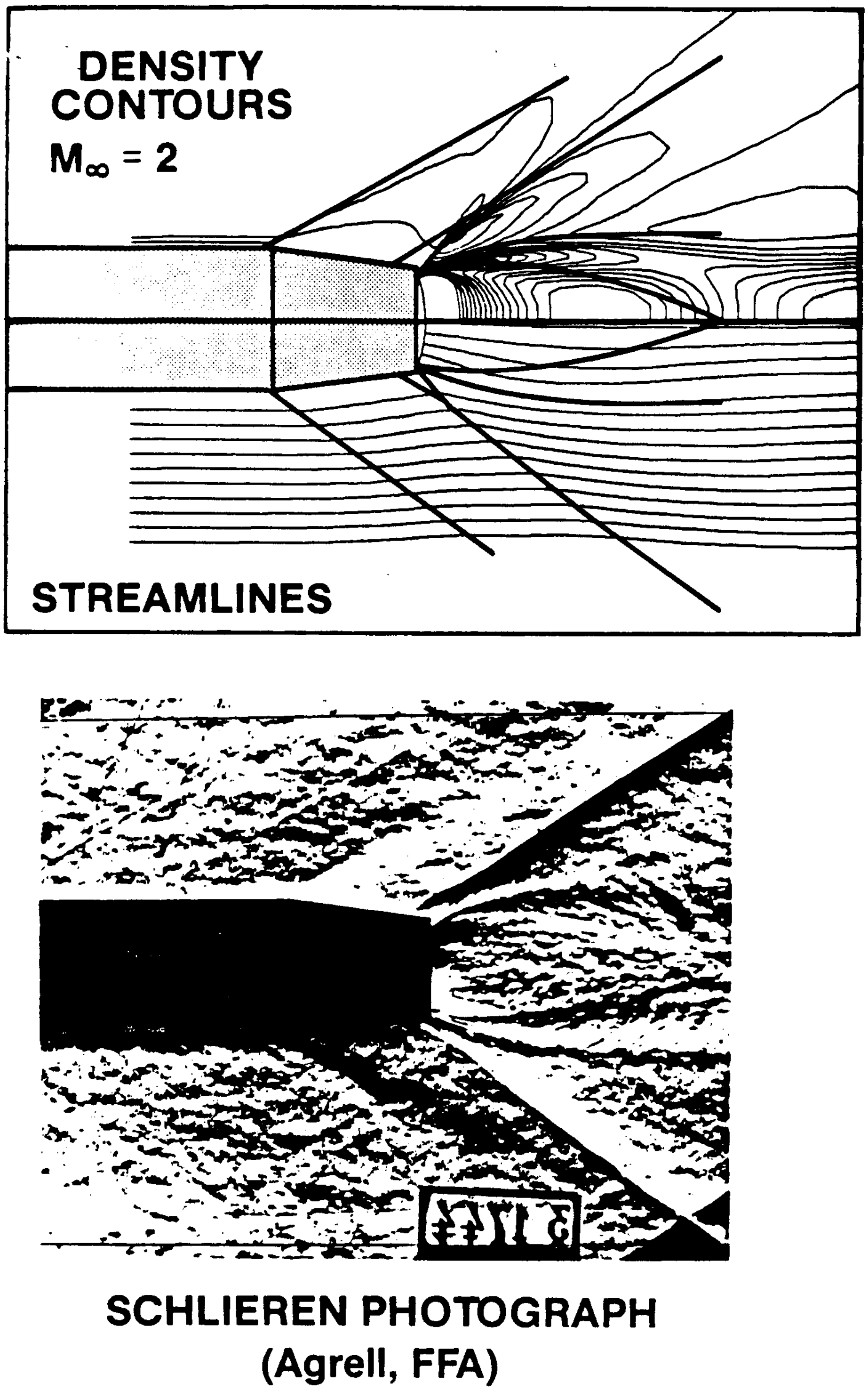

FIGURE 35. Boattail Exhaust Plume Flow Details at Pressure Ratio = 3.

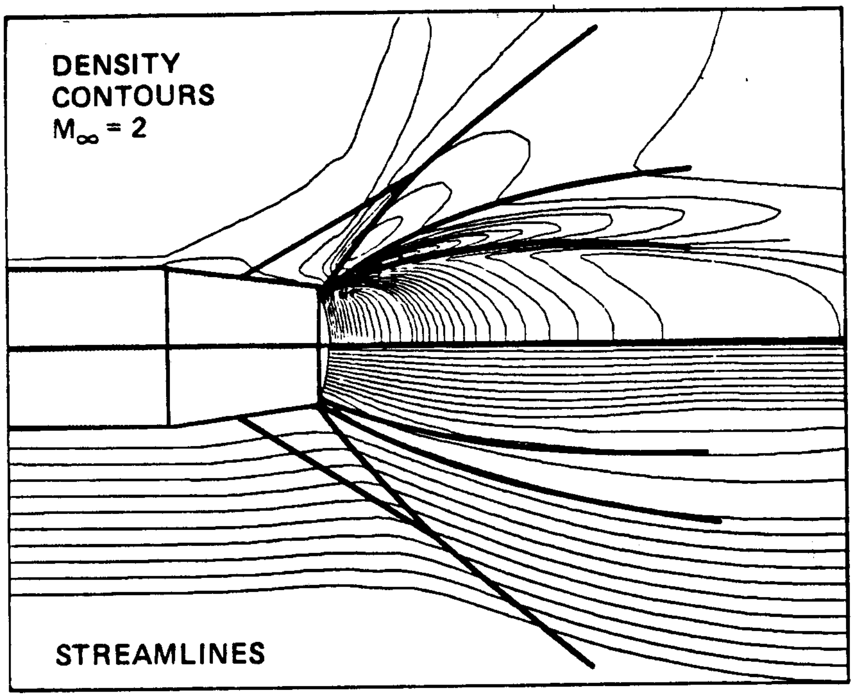

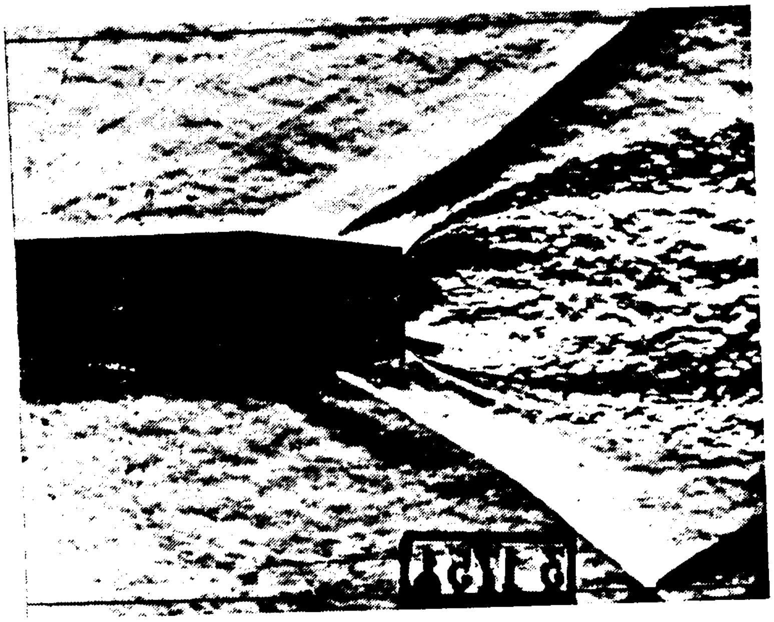

SCHLIEREN PHOTOGRAPH
(Agrell, FFA)

FIGURE 36. Boattail Exhaust Plume Flow Details at Pressure Ratio = 9.